Control Strategues for Automatic Generation Control over MTDC Grid

McNamara, P., Meere, R., O'Donnell, T., & McLoone, S. (2016). Control Strategues for Automatic Generation Control over MTDC Grid. *Control Engineering Practice*, *54*, 129-139.
https://doi.org/10.1016/j.conengprac.2016.05.016

Published in:
Control Engineering Practice

Document Version:
Peer reviewed version

Queen's University Belfast - Research Portal:
Link to publication record in Queen's University Belfast Research Portal

Control Strategies for Automatic Generation Control over MTDC Grids

Paul Mc Namara[a,1], Ronan Meere[b], Terence O'Donnell[b], Seán McLoone[c]

[a]*Maynooth University Electronic Engineering Dept., Callan Institute, NUI Maynooth, Maynooth, Kildare, Ireland.*
[b]*Electricity Research Centre, Engineering & Materials Science Centre, University College Dublin, Belfield, Dublin 4, Ireland.*
[c]*Energy, Power and Intelligent Control Research Cluster, School of Electronics, Electrical Engineering and Computer Science, Queens University Belfast, Belfast, Northern Ireland.*

Abstract

Increasingly in power systems, there is a trend towards the sharing of reserves and integration of markets over wide areas in order to enable increased penetration of renewable sources in interconnected power systems. In this paper, a number of simple PI and gain based Model Predictive Control algorithms are proposed for Automatic Generation Control in AC areas connected to Multi Terminal Direct Current grids. The paper discusses how this approach improves the sharing of secondary reserves and could assist in achieving EU energy targets for 2030 and beyond.

Keywords: Multi-terminal HVDC, Model Predictive Control, Automatic Generation Control, Supergrid.

List of abbreviations

AC: Alternating Current
AGC: Automatic Generation Control
CMPC: Centralised MPC
DC: Direct Current
HVDC: High Voltage Direct Current
MPC: Model Predictive Control
MTDC: Multi-Terminal HVDC
(controller)-NVO: Controller with No Voltage Offsets
PFC: Primary Frequency Control
ROCOF: Rate Of Change Of Frequency
SMPC: Selfish MPC
VSC: Voltage Source Converter
(controller)-WVO: Controller With Voltage Offsets

1. Introduction

It is recognised that a significantly higher share of renewable energy production is necessary to improve the competitiveness, security, and sustainability of energy systems across the world. Reflecting this, for example, the EU has set a goal of 27% renewable energy penetration, to be achieved collectively across Europe by 2030, which is an increase of 7% on the 2020 target (European Commission, 2014). However, stochastic, intermittent sources such as wind and solar can cause issues from a grid reliability perspective, and usually the areas most suited to the harvesting of such renewables are located far away from the location of the largest loads. By sharing these sources over a wide area, the stochasticity of the individual sources can be aggregated, improving the overall predictability and stability of the energy supply. Thus the development of suitable transmission networks is vital for the integration of these renewables (European Commission, 2014; Houghton et al., 2012). In Europe, an interconnected grid or "Supergrid" which would facilitate access to variable renewable sources across the continent, such as wind from the North of Europe and solar from the South of Europe and North Africa, has thus received widespread attention (Van Hertem and Ghandhari, 2010). In particular, the North Sea offshore grid is of note, where the combination of the large offshore wind capacity in this area and the hydro storage capacity available in Norway make it a likely candidate as a starting point for Europe's first offshore DC grid (Spro et al., 2014; Chaudhuri et al., 2014).

High Voltage Direct Current (HVDC) transmission facilitates the transfer of large quantities of electrical power over long distances by utilising Direct Current (DC) power transmission (Kundur, 1994). Most HVDC lines are point-to-point lines that transfer energy between only two Alternating Current (AC) areas, with a converter on each side. Modern Voltage Source Converter (VSC) based HVDC technologies allow a number of HVDC lines to be connected to a single DC grid terminal (de Courreges d'Ustou, 2012). Thus Multi-Terminal HVDC (MTDC) grids can be constructed, which consist of a radial or meshed HVDC grid with a number of connections to AC grids. Consequently, this facilitates the sharing of energy reserves over large areas and subsequently there has been much interest in developing coordinated control methods which allow power injections to and from the MTDC grid to support frequency control in connected AC areas. The world's

Email address: paul.mcnamara@ucd.ie (Paul Mc Namara)
[1]Present address: Electricity Research Centre, Engineering & Materials Science Centre, University College Dublin, Belfield, Dublin 4, Ireland.

This preprint has been accepted for publication in Control Engineering Practice

first VSC-based MTDC grid, the Zhoushan MTDC grid in China, was put into operation in July 2014 (Tang et al., 2015).

A number of primary control algorithms, which operate on the milliseconds to seconds scale, and secondary control algorithms, which act on the seconds to minutes scale, have been developed for MTDC grids, typically for the regulation of the voltages and DC grid power transfers (Hendriks et al., 2007; Beerten and Belmans, 2013; Egea-Alvarez et al., 2013; Arags-Pealba et al., 2014; Egea-Alvarez et al., 2012; Zonetti et al., 2014; Andreasson et al., 2013). A range of primary control algorithms exist for sharing power between areas. Techniques such as voltage margin control, droop control, ratio and priority control are used to regulate both the DC voltages and power transfers on the DC grid. In addition to these fixed controllers, adaptive droop controllers have been developed that incorporate the remaining reserves in an area into the droop gain calculation for that area, so as to adaptively change the primary reserve contributions of a particular HVDC terminal (Chaudhuri et al., 2014).

Primary Frequency Control (PFC) algorithms have also been proposed for the sharing of primary reserves over MTDC grids in order to collectively regulate the frequencies in AC connected areas (Wiget et al., 2015; Silva et al., 2012; Dai et al., 2012; Chaudhuri et al., 2013). Communication based PFC methods can be non-robust to communication delays or failures (Dai et al., 2010) and hence a number of droop methods that do not rely on communication between areas have been proposed. These operate by manipulating the DC voltages on the grid in a decentralised fashion in order to regulate the power flows into or out of AC areas and the MTDC grid.

As with the case of decentralised PFC in AC areas, it is necessary to provide secondary frequency control, usually referred to as Automatic Generation Control (AGC) so as to satisfy long-term frequency regulation goals across areas connected to MTDC grids. A number of decentralised PI-based AGC strategies have been proposed previously for MTDC systems in (Dai, 2011; Chaudhuri et al., 2014), while a centrally optimised PID-based method was proposed in (de Courreges d'Ustou, 2012).

Model Predictive Control (MPC) (Maciejowski, 2002) algorithms enable the optimal control of a system based on the use of state-space predictions. MPC has been used previously for the control of HVDC systems (Fuchs et al., 2014; Mariethoz et al., 2014; Azad et al., 2013) and has also been applied to power systems for AGC (Ersdal et al., 2015, 2016; Ma et al., 2014; Wang et al., 2014; Mohamed et al., 2012; Shiroei and Ranjbar, 2014; Shiroei et al., 2013). There are a number of advantages to the use of MPC versus PI controllers. MPC offers a systematic methodology for handling the control of MIMO systems. Control is implemented via the minimisation of a weighted sum of different cost functions which represent the various control goals of the system. As a result the tuning of MPC controllers is highly intuitive as users have only to change the weights assigned to each of these goals to achieved the desired performance. As MPC is based on optimisation, constraints can be systematically included in the control formulation. While MPC can be susceptible to problems such as model uncertainty and noise, it typically offers improved robustness in comparison to PI controllers. Finally, once an MPC framework has been derived for the control of a system, it is possible then to combine a vast range of techniques from both the control and optimisation literature in order to control the system as desired.

Given the widespread use of linear analysis in power systems, it is desirable to develop linear MPC algorithms for use in power systems. Thus in this paper, a number of simplified linear gain based MPC controllers are proposed for use with AGC for MTDC grids. Also, by keeping these algorithms as simple as possible it encourages their adoption by industry based practitioners.

The use of additional secondary voltage offsets is also investigated in this paper. These act as a means of improving the control of DC voltages on a long-term basis, thus giving TSOs increased flexibility in terms of how secondary reserves may be shared between AC areas, with the aim of improving the efficiency with which secondary reserves are used over the entire electrical grid.

Thus the following controllers are proposed for the control of the MTDC system:

- Firstly, decentralised PI controllers With Voltage Offsets (PI-WVO) and decentralised PI controllers with No Voltage Offsets (PI-NVO) are considered (hereafter WVO and NVO will be used to denote controllers with and without voltage offsets, respectively).
- Then, two Centralised MPC (CMPC) controllers, CMPC-WVO and CMPC-NVO are designed.
- Finally, based on the centralised MPC design two decentralised Selfish MPC (SMPC) controllers, SMPC-WVO and SMPC-NVO are derived.

The proposed MPC design approaches for AC frequency control of areas connected to the DC grid are, to the authors best knowledge, novel.

The remainder of the paper is organised as follows; the modelling and PFC of the MTDC grid is presented in Section 2, and the PI based strategies for AGC are introduced in Section 3. The centralised and decentralised MPC approaches are introduced in Sections 4 and 5, respectively. Section 6 then shows how AGC can be achieved using MPC. Results of a simulation study are given in Section 8 and, finally, conclusions are presented in Section 9.

2. Modelling and Primary Frequency Control for Multi-Terminal HVDC grids

A MTDC grid is composed of a DC grid and N AC areas, each with a converter which serves as an interface for transferring power to and from the DC grid, as in Fig. 1

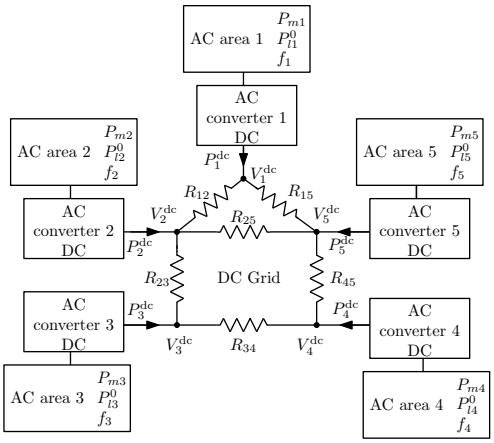

Figure 1: A multi-terminal DC grid connecting $N = 5$ AC areas via converters (Sarlette et al., 2012).

(Sarlette et al., 2012). Each AC area i, for $i = 1, 2, \ldots, N$, has a state vector $(f_i, P_{\mathrm{m}i}) \in \Re^2$, and is governed by the following dynamic equations:

$$\dot{f}_i(t) = \frac{P_{\mathrm{m}i}(t) - P_{\mathrm{l}i}(t) - P_i^{\mathrm{dc}}(t)}{4\pi^2 J_i f_i(t)} - \frac{D_{\mathrm{g}i}}{J_i}(f_i(t) - \bar{f}_i), \quad (1)$$

$$\dot{P}_{\mathrm{m}i}(t) = \frac{1}{\tau_{\mathrm{m}i}}(P^0_{\mathrm{m}i}(t) - P_{\mathrm{m}i}(t)) - \frac{P_{\mathrm{nom},i}}{\sigma_i \tau_{\mathrm{m}i}} \frac{f_i(t) - \bar{f}_i}{\bar{f}_i}, \quad (2)$$

$$P_{\mathrm{l}i}(t) = P^0_{\mathrm{l}i}(t)(1 + D_{\mathrm{l}i}(f_i(t) - \bar{f}_i)), \quad (3)$$

where J_i is the moment of inertia of aggregated area i (kg m^2), $f_i(t)$ is the frequency (Hz), $P_{\mathrm{m}i}(t)$ is the mechanical power (W), $P_{\mathrm{l}i}(t)$ is the load disturbance considering frequency effects (W), $P_i^{\mathrm{dc}}(t)$ is the DC power AC area i is injecting into the DC grid (W), $D_{\mathrm{g}i}$ is the damping factor (W s^2), $\tau_{\mathrm{m}i}$ is the time constant for power adjustment (s), $P^0_{\mathrm{m}i}(t)$ is the reference mechanical power which is manipulated using AGC (W), σ_i is the generator droop (dimensionless), $P^0_{\mathrm{l}i}(t)$ is the nominal load disturbance at bus i (W), and $D_{\mathrm{l}i}$ is the sensitivity of $P_{\mathrm{l}i}(t)$ to deviations of the frequency from the nominal operating frequency $\bar{f}_i$ (s) (Kundur, 1994). In this paper, for a general variable b, $\bar{b}$ denotes the operating point of this variable at equilibrium.

The dynamics of the HVDC converters are not significant at the time scales considered in this work and hence associated variables are assumed to be at their steady state values. It is assumed that the power entering the DC grid equals that leaving it, i.e.,

$$P_1^{\mathrm{dc}}(t) + \ldots + P_N^{\mathrm{dc}}(t) = 0. \quad (4)$$

A positive $P_i^{\mathrm{dc}}(t)$ indicates area i is injecting P_i^{dc} W into the HVDC grid, and a negative $P_i^{\mathrm{dc}}(t)$ indicates area i is receiving P_i^{dc} W from the HVDC grid. Denoting $V_i^{\mathrm{dc}}(t)$ as the DC voltage of area i, it follows that,

$$P_i^{\mathrm{dc}}(t) = \sum_{j=1}^{N} \frac{V_i^{\mathrm{dc}}(t)(V_i^{\mathrm{dc}}(t) - V_j^{\mathrm{dc}}(t))}{R_{ij}}, \quad (5)$$

where $R_{ij} = R_{ji}$ is the resistance in the HVDC line connecting areas i and j, and $R_{ij} = \infty$ if areas i and j are not connected by a DC line.

A communication-free decentralised PFC law was proposed for the sharing of primary reserves amongst AC areas over the HVDC network in (Sarlette et al., 2012). This is given by

$$v_i = \gamma_i x_{\mathrm{f}i}, \quad (6)$$

where $v_i(t)$ is the DC input voltage deviation at area i ($v_i(t) = V_i^{\mathrm{dc}}(t) - \bar{V}_i^{\mathrm{dc}}$), the state $x_{\mathrm{f}i}$ is the frequency deviation of area i ($x_{\mathrm{f}i} = f_i(t) - \bar{f}_i$), and γ_i is the DC voltage PFC gain of the i-th agent. This controller allows the DC voltages to respond in real time to frequency deviations, where manipulation of these voltages results in a power exchange with the DC grid according to (5). Thus increases in frequency result in increases in the power supplied to the DC grid, and vice-versa, thereby supporting frequency regulation according to (1). This control law effectively shares resources amongst AC areas and the conditions for stable control under this law are given in (Sarlette et al., 2012). In this paper each of the NVO scenarios considered use this primary controller alone for manipulation of the DC link voltages.

3. PI-based AGC for Multi-terminal HVDC grids

The objective of AGC in area i is to maintain the frequency within the area at its scheduled value, $\bar{f}_i$. Usually, maintenance of the net interchange power with connected areas, $\bar{P}_i^{\mathrm{dc}}$, will also be included in the AGC objective. It may also be desirable to minimise the Rate Of Change Of Frequency (ROCOF) (Tielens and Van Hertem, 2012). Control algorithms for AGC are then designed and tuned so as to balance these three objectives.

Previously in the MTDC literature AGC has been performed via manipulation of $P^0_{\mathrm{m}i}(t)$ alone (Dai, 2011; Mc Namara et al., 2014). In this case positive deviations in either f_i or $P_i^{\mathrm{dc}i}$ are regulated by decreasing $P^0_{\mathrm{m}i}$, and negative deviations in f_i or $P_i^{\mathrm{dc}i}$ are regulated by increasing $P^0_{\mathrm{m}i}$. For a simple continuous-time PI-based controller, $P^0_{\mathrm{m}i}(t)$, is manipulated as follows:

$$u_{\mathrm{P}i} = -\chi_{\mathrm{m}i} \int (\beta_i x_{\mathrm{f}i} + \eta_i z_i) \mathrm{d}t, \quad (7)$$

where $u_{\mathrm{P}i}(k) = P^0_{\mathrm{m}i}(k) - \bar{P}^0_{\mathrm{m}i}$, $\chi_{\mathrm{m}i}$ is the non-negative mechanical power integral gain coefficient, β_i is a frequency weighting coefficient, η_i is a binary variable that is set to 1 if the scheduled DC power injections from an area being regulated, and 0 otherwise, and $z_i(k) = P_i^{\mathrm{dc}}(k) - \bar{P}_i^{\mathrm{dc}}$. In accordance with (Kundur, 1994), β_i is calculated as:

$$\beta_i = \frac{1}{\sigma_i} + D_{\mathrm{g}i}. \quad (8)$$

In this paper the voltage offset, $V_{\mathrm{dc}i}^{\mathrm{os}}(t)$, is introduced in order to improve the control of the DC line power flows as follows:

$$v_i = V_{\mathrm{dc}i}^{\mathrm{os}}(t) + \gamma_i x_{\mathrm{f}i}. \quad (9)$$

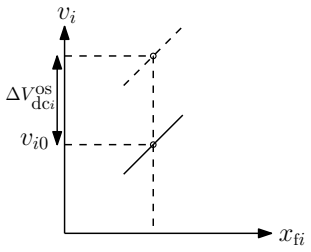

Figure 2: Droop response of DC voltage, illustrating the effect on the relationship between v_i and $x_{\mathrm{f}i}$ when a secondary DC voltage $\Delta V_{\mathrm{dc}i}^{os}$ is applied to the system.

The effect on the relationship between v_i and $x_{\mathrm{f}i}$ of applying the secondary DC voltage offset is illustrated in Fig. 2. The following PI-based strategy is proposed for determining the voltage offset:

$$V_{\mathrm{dc}i}^{\mathrm{os}}(t) = \chi_{\mathrm{dc}i} \int (\beta_i x_{\mathrm{f}i} - \eta_i z_i)\mathrm{d}t, \tag{10}$$

where $\chi_{\mathrm{dc}i}$ is the non-negative DC power integral gain coefficient. The same logic that was used in the design of the primary frequency controller, given by (6), applies here too. The same weighting structure between the frequency and DC power is chosen here as in (8) in order to simplify tuning and encourage a coherent response between the voltages and the mechanical powers. Hence, for the purposes of this paper the PI-NVO algorithm uses only (7) for secondary control of the mechanical powers, while the PI-WVO algorithm uses both (7) and (10) together to simultaneously manipulate mechanical powers and DC voltages for AGC purposes.

These PI strategies are very simple decentralised algorithms that require no communication between areas. It is of interest then to investigate more complex optimal and centralised control algorithms, to see if they can provide improved performance over the PI algorithms. In this context, in the following sections novel centralised and decentralised Model Predictive Control algorithms for AGC are introduced.

4. Model Predictive Control

Model Predictive Control is an optimisation based control technique that uses state-space based predictions in order to form optimal inputs to a system over a prediction horizon. While inputs are calculated over the full prediction horizon, only the input for the first sample step of the prediction horizon is applied to the system, and this process is repeated every sample step.

Consider a system consisting of n non-overlapping subsystems. A discrete-time, linear, time-invariant state-space model for this system is given by

$$\boldsymbol{x}(k+1) = \boldsymbol{A}\boldsymbol{x}(k) + \boldsymbol{B}\boldsymbol{u}(k) \tag{11}$$

$$\boldsymbol{y}(k) = \boldsymbol{C}\boldsymbol{x}(k), \tag{12}$$

where $\boldsymbol{x}(k)=[\boldsymbol{x}_1^{\mathrm{T}}(k),\ldots,\boldsymbol{x}_n^{\mathrm{T}}(k)]^{\mathrm{T}}$, $\boldsymbol{u}(k)=[\boldsymbol{u}_1^{\mathrm{T}}(k),\ldots,\boldsymbol{u}_n^{\mathrm{T}}(k)]^{\mathrm{T}}$, and $\boldsymbol{y}(k) = [\boldsymbol{y}_1^{\mathrm{T}}(k),\ldots,\boldsymbol{y}_n^{\mathrm{T}}(k)]^{\mathrm{T}}$, and $\boldsymbol{x}_a(k)$, $\boldsymbol{u}_a(k)$, and $\boldsymbol{y}_a(k)$ are the states, inputs, and outputs of subsystem a at sample step k, respectively. Matrices $\boldsymbol{A}$, $\boldsymbol{B}$, and $\boldsymbol{C}$ are the relevant state-space matrices. An augmented state-space model allows these equations to be framed in terms of $\Delta\boldsymbol{u}(k)$ and the augmented state $\boldsymbol{\chi}(k)=[\Delta\boldsymbol{x}^{\mathrm{T}}(k)\ \boldsymbol{x}^{\mathrm{T}}(k)]^{\mathrm{T}}$ (for a general variable $b(k)$, $\Delta b(k)=b(k)-b(k-1)$, i.e., the Δ operator denotes the change in a variable between sample steps $k-1$ and k), which ensures integral action in the controller. This is given as follows:

$$\boldsymbol{\chi}(k+1) = \hat{\boldsymbol{A}}\boldsymbol{\chi}(k) + \hat{\boldsymbol{B}}\Delta\boldsymbol{u}(k) \tag{13}$$

$$\boldsymbol{y}(k+1) = \hat{\boldsymbol{C}}\boldsymbol{\chi}(k+1), \tag{14}$$

where $\hat{\boldsymbol{A}}$, $\hat{\boldsymbol{B}}$, $\hat{\boldsymbol{V}}$, and $\hat{\boldsymbol{C}}$ are the incremental state-space matrices. The predicted state $\tilde{\boldsymbol{x}}(k+1)$ and incremental predicted state $\Delta\tilde{\boldsymbol{x}}(k+1)$ can be found from these equations, where for a general vector $\boldsymbol{p}$, its prediction vector is $\tilde{\boldsymbol{p}}(k) = [\boldsymbol{p}^{\mathrm{T}}(k)\ldots\boldsymbol{p}^{\mathrm{T}}(k+H-1)]^{\mathrm{T}}$, where H is called the prediction horizon for the system(Maciejowski, 2002).

MPC problems are constructed to fulfill control objectives for a system based on knowledge of $\boldsymbol{x}(k)$. A cost function, $J(\boldsymbol{\chi}(k),\Delta\tilde{\boldsymbol{u}}(k))$ (which will henceforth be denoted by $J(k)$), is designed so as to embody the system's objectives. Typically this cost function is quadratic in $\Delta\tilde{\boldsymbol{u}}$ and in this paper the cost function takes the following form:

$$\begin{aligned} J(k) =& \tilde{\boldsymbol{e}}^{\mathrm{T}}\boldsymbol{Q}_{\mathrm{e}}\tilde{\boldsymbol{e}} + \Delta\tilde{\boldsymbol{x}}^{\mathrm{T}}\boldsymbol{Q}_{\mathrm{x}}\Delta\tilde{\boldsymbol{x}} + \Delta\tilde{\boldsymbol{u}}^{\mathrm{T}}\boldsymbol{Q}_{\mathrm{u}}\Delta\tilde{\boldsymbol{u}} \\ =& \Delta\tilde{\boldsymbol{u}}^{\mathrm{T}}\boldsymbol{G}\Delta\tilde{\boldsymbol{u}} + \Delta\tilde{\boldsymbol{u}}^{\mathrm{T}}\boldsymbol{f} + \mu, \end{aligned} \tag{15}$$

where the $(k+1)$ dependency is dropped from $\tilde{\boldsymbol{e}}(k+1)$ and $\Delta\tilde{\boldsymbol{x}}(k+1)$, and the (k) dependency is dropped from $\Delta\tilde{\boldsymbol{u}}(k)$ in (15) for compactness. The error vector, $\boldsymbol{e}(k) = [\boldsymbol{e}_1^{\mathrm{T}}(k),\ldots,\boldsymbol{e}_n^{\mathrm{T}}(k)]^{\mathrm{T}}$, where $\boldsymbol{e}_a(k)=\boldsymbol{y}_a(k)-\boldsymbol{r}_a(k)$ and $\boldsymbol{r}_a(k)$ are the setpoints of subsystem a at sample step k. The second term in the cost function $\Delta\tilde{\boldsymbol{x}}^{\mathrm{T}}\boldsymbol{Q}_{\mathrm{x}}\Delta\tilde{\boldsymbol{x}}=\tilde{\boldsymbol{\chi}}^{\mathrm{T}}\boldsymbol{Q}_{\chi}\tilde{\boldsymbol{\chi}}$, where $\boldsymbol{Q}_{\chi}$ is constructed so as to satisfy the aforementioned equality. Following straightforward matrix manipulation it can be shown that $\boldsymbol{G} = \hat{\boldsymbol{B}}^{\mathrm{T}}\hat{\boldsymbol{C}}^{\mathrm{T}}\boldsymbol{Q}_{\mathrm{e}}\hat{\boldsymbol{C}}\hat{\boldsymbol{B}} + \hat{\boldsymbol{B}}^{\mathrm{T}}\boldsymbol{Q}_{\mathrm{x}}\hat{\boldsymbol{B}} + \hat{\boldsymbol{Q}}_{\mathrm{u}}$, where $\boldsymbol{G}$ is a square symmetric non-singular matrix, $\boldsymbol{f} = \boldsymbol{K}_{\chi}\boldsymbol{\chi}(k) - \boldsymbol{K}_{\mathrm{r}}\tilde{\boldsymbol{r}}(k)$, where $\boldsymbol{K}_{\chi} = 2\hat{\boldsymbol{B}}^{\mathrm{T}}\hat{\boldsymbol{C}}^{\mathrm{T}}\boldsymbol{Q}_{\mathrm{e}}\hat{\boldsymbol{C}}\hat{\boldsymbol{A}} + \hat{\boldsymbol{B}}^{\mathrm{T}}\boldsymbol{Q}_{\mathrm{x}}\boldsymbol{A}$ and $\boldsymbol{K}_{\mathrm{r}} = 2\hat{\boldsymbol{B}}^{\mathrm{T}}\hat{\boldsymbol{C}}^{\mathrm{T}}\boldsymbol{Q}_{\mathrm{e}}$ are constant matrices. The constant μ represents terms that do not depend on $\Delta\tilde{\boldsymbol{u}}(k)$.

The weighting matrices $\boldsymbol{Q}_{\mathrm{e}}$, $\boldsymbol{Q}_{\mathrm{x}}$, and $\boldsymbol{Q}_{\mathrm{u}}$ determine the relative importance of minimising errors, the incremental changes in states, and the incremental changes in inputs, respectively. For the unconstrained case, an analytical solution for the inputs can then be found by finding the value of $\Delta\tilde{\boldsymbol{u}}(k)$ that minimises $J(k)$.

The optimal choice of controls $\Delta\tilde{\boldsymbol{u}}^*(k)$ is obtained when,

$$\frac{\partial}{\partial\Delta\tilde{\boldsymbol{u}}(k)}J(k) = 2\boldsymbol{G}\Delta\tilde{\boldsymbol{u}}(k) + \boldsymbol{f} = 0, \tag{16}$$

where a superscripted * denotes the optimum value of a variable. This yields the solution,

$$\begin{aligned}\Delta\tilde{\boldsymbol{u}}^*(k) &= -\frac{1}{2}\boldsymbol{G}^{-1}\boldsymbol{f} \\ &= -\frac{1}{2}\boldsymbol{G}^{-1}(\boldsymbol{K}_{\chi}\boldsymbol{\chi}(k) - \boldsymbol{K}_{\mathrm{r}}\tilde{\boldsymbol{r}}(k))\end{aligned} \tag{17}$$

Thus the control law is effectively a fixed gain feedback law and can be computed in a highly efficient fashion. The input at the start of the horizon $\boldsymbol{u}(k)$ is applied to the system and this process is repeated each sample step. Unconstrained MPC in this form is equivalent in performance to a Finite Horizon Linear Quadratic Regulator.

Previously, PI-based AGC for MTDC has been implemented in a decentralised fashion (Dai, 2011). Thus it is of interest to investigate the performance of a decentralised MPC controller too. This is described in the following section.

5. Decentralised SMPC

The SMPC algorithm is described in this section. A discrete-time, linear, time-invariant state-space model is used to model the dynamics of each subsystem,

$$\boldsymbol{x}_a(k+1) = \boldsymbol{A}_a\boldsymbol{x}_a(k) + \boldsymbol{B}_a\boldsymbol{u}_a(k) \tag{18}$$

$$\boldsymbol{y}_a(k) = \boldsymbol{C}_a\boldsymbol{x}_a(k), \tag{19}$$

where the matrices $\boldsymbol{A}_a$, $\boldsymbol{B}_a$, and $\boldsymbol{C}_a$ are the relevant state-space matrices. As in the centralised case the state-space is augmented to give the equations in terms of $\Delta\boldsymbol{u}_a(k)$ and the augmented state $\boldsymbol{\chi}_a(k)=[\Delta\boldsymbol{x}_a^{\mathrm{T}}(k)\ \boldsymbol{x}_a^{\mathrm{T}}(k)]^{\mathrm{T}}$, and these state-space equations can then be used to find $\Delta\tilde{\boldsymbol{x}}_a(k+1)$ and $\tilde{\boldsymbol{x}}_a(k+1)$. The decentralised SMPC algorithm presented here bases its control only on local measurements, and its predictions on local state-space matrices. Hence, the local cost function at sample step k, $J_a^{\mathrm{local}}(k)$, is defined as:

$$J_a^{\mathrm{local}}(k) = \tilde{\boldsymbol{e}}_a^{\mathrm{T}}\boldsymbol{Q}_{\mathrm{e}a}\tilde{\boldsymbol{e}}_a + \Delta\tilde{\boldsymbol{x}}_a^{\mathrm{T}}\boldsymbol{Q}_{\mathrm{x}a}\Delta\tilde{\boldsymbol{x}}_a + \Delta\tilde{\boldsymbol{u}}_a^{\mathrm{T}}\boldsymbol{Q}_{\mathrm{u}a}\Delta\tilde{\boldsymbol{u}}_a, \tag{20}$$

where the $(k+1)$ dependency is dropped from $\tilde{\boldsymbol{e}}_a$ and $\Delta\tilde{\boldsymbol{x}}_a$, and the (k) dependency is dropped from $\Delta\tilde{\boldsymbol{u}}_a$ for compactness. The weighting matrices $\boldsymbol{Q}_{\mathrm{e}a}$, $\boldsymbol{Q}_{\mathrm{x}a}$, and $\boldsymbol{Q}_{\mathrm{u}a}$ determine the relative importance of minimising the local errors, the local incremental changes in states, and the local incremental changes in inputs, respectively. Since the local cost function is quadratic, it follows that in the absence of inequality constraints a simple feedback control law can be derived analytically for each subsystem (local area) as in (17).

6. Automatic Generation Control using MPC in MTDC systems

The method for implementing AGC using MPC is now described. In the following, for conciseness only the derivation of the WVO approach is presented. The NVO implementation can be obtained in a similar fashion either by omitting the voltage offset parts, or setting the voltage offset to 0.

Assuming a discrete-time controller for AGC, at sample step k, the objective function for area i, $\Psi_i(k)$, is given by

$$\begin{aligned}\Psi_i(k) =& Q_{\mathrm{f}i}x_{\mathrm{f}i}^2(k+1) + Q_{\mathrm{z}i}z_i^2(k+1) + Q_{\mathrm{df}i}\Delta x_{\mathrm{f}i}^2(k+1) \\ &+ Q_{\mathrm{dP}i}\Delta u_{\mathrm{P}i}^2(k) + Q_{\mathrm{dv}i}\Delta u_{\mathrm{v}i}^2(k),\end{aligned} \tag{21}$$

where $u_{\mathrm{v}i}(k)=V_{\mathrm{dc}i}^0(k)-\bar{V}_{\mathrm{dc}i}^0$. The variables $Q_{\mathrm{f}i}$, $Q_{\mathrm{z}i}$, $Q_{\mathrm{df}i}$, $Q_{\mathrm{dP}i}$, and $Q_{\mathrm{dv}i}$ are weights which determine the relative importance of minimising $x_{\mathrm{f}i}^2(k+1)$, $z_i^2(k+1)$, $\Delta x_{\mathrm{f}i}^2(k+1)$, $\Delta u_{\mathrm{P}i}^2(k)$, and $\Delta u_{\mathrm{v}i}^2(k)$, respectively. The first 3 terms in (21) are concerned with fulfilling the power system objectives of minimising frequency deviations about $\bar{f}_i$, maintaining scheduled DC power flows into the HVDC grid, and minimising the ROCOF. The final 2 terms are stabilising terms that can be used to tune the control performance of the system, by discouraging large changes in the inputs from occuring sample to sample.

Before deriving the linear state-space equations for AGC, the technique for adding voltage offsets to the DC link when using MPC is outlined for the WVO scenarios. The secondary voltage offsets are still added to the primary voltage controller as in (9). However, in order to ensure smooth control actions for a discrete-time secondary controller, $V_{\mathrm{dc}i}^{\mathrm{os}}(t)$ is designed to have the following dynamic response:

$$\dot{V}_{\mathrm{dc}i}^{\mathrm{os}}(t) = \frac{1}{\tau_{\mathrm{dc}i}}\left(V_{\mathrm{dc}i}^0(t) - V_{\mathrm{dc}i}^{\mathrm{os}}(t)\right), \tag{22}$$

where $V_{\mathrm{dc}i}^{\mathrm{os}}(t)$ is the setpoint for the secondary DC voltage offset control, and $\tau_{\mathrm{dc}i}$ is a time constant in seconds which is specified by the user in order to determine the speed of the response of $V_{\mathrm{dc}i}^{\mathrm{os}}(t)$. Thus the setpoints $P_{\mathrm{m}i}^0(t)$ and $V_{\mathrm{dc}i}^0(t)$ are manipulated for the purposes of AGC.

The $\tau_{\mathrm{dc}i}$ time constant can effectively be tuned depending on the speed with which practitioners desire the secondary DC voltage offset to enter the system. From a practical perspective designers should choose this parameter such that the discretised model used for MPC accurately tracks the continuous-time trajectory of the secondary DC voltage offset. From the authors' experience, once this is taken into consideration the $\tau_{\mathrm{dc}i}$ parameters can be considered independently at each terminal without affecting the stability of the system. Also it should be noted that as values of $\tau_{\mathrm{dc}i}$ become smaller this in turn results in more step-like DC power inputs into the system, which may be undesirable from a frequency control perspective in terms of minimising the ROCOF or introducing undesirable harmonics into the system response. Thus longer values of $\tau_{\mathrm{dc}i}$ imply "smoother" frequency responses.

In order to develop a linear cost function to implement MPC for AGC, it is necessary to linearise equations (1) and (5), in order to generate state predictions. These linearisations are given as follows, as in (Dai, 2011):

$$\dot{x}_{\mathrm{f}i} = \frac{P_{\mathrm{m}i}(t) - P_{\mathrm{l}i}(t) - P_i^{\mathrm{dc}}(t)}{4\pi^2\bar{f}_iJ_i} - \frac{D_{\mathrm{g}i}}{J_i}x_{\mathrm{f}i}, \tag{23}$$

$$z_i = \sum_{j=1}^{N} \frac{\bar{V}_i^{\rm dc}(v_i - v_j)}{R_{ij}}. \tag{24}$$

In order to incorporate z_i into the state-space, an equation for $\dot{z}_i$ must be derived. This is given by:

$$\begin{aligned} \dot{z}_i &= \sum_{j=1}^{N} \frac{\bar{V}_i^{\rm dc}(\dot{v}_i - \dot{v}_j)}{R_{ij}} \\ &= \sum_{j=1}^{N} \frac{\bar{V}_i^{\rm dc}(\dot{V}_{{\rm dc}i}^{\rm os}(t) + \gamma_i \dot{x}_{{\rm f}i} - \dot{V}_{{\rm dc}j}^{\rm os}(t) - \gamma_j \dot{x}_{{\rm f}j})}{R_{ij}}, \end{aligned} \tag{25}$$

where in turn $\dot{V}_{{\rm dc}i}^{\rm os}(t)$ and $\dot{x}_{{\rm f}i}$ are given by (22) and (23), respectively.

The state-space equations (2), (22), (23), and (25) are then used to describe the dynamics of the system about an operating point where the state of agent i is given by $\boldsymbol{x}_i = [x_{{\rm f}i}, x_{{\rm P}i}, x_{{\rm v}i}, z_i]^{\rm T}$. Here, $x_{{\rm P}i} = P_{{\rm m}i}(t) - \bar{P}_{{\rm m}i}$ and $x_{{\rm v}i} = V_{{\rm dc}i}^{\rm os}(t) - \bar{V}_{{\rm dc}i}^{\rm os}$ are the mechanical power and DC voltage deviations about the operating point, respectively. The input to agent i is given by $\boldsymbol{u}_i = [u_{{\rm P}i}, u_{{\rm v}i}]^{\rm T}$, and its output by $\boldsymbol{y}_i = \boldsymbol{C}_i \boldsymbol{x}_i$. When only the frequency is being regulated $y_i = x_{{\rm f}i}$, and when DC power regulation is enforced $\boldsymbol{y}_i = [x_{{\rm f}i}, z_i]^{\rm T}$. The matrix $\boldsymbol{C}$ is then chosen accordingly, depending on which case is being considered. Each subsystem is then allocated its own control agent. Using state-space predictions each agent generates a local cost function:

$$J_i^{\rm local}(k) = \sum_{p=k}^{k+H-1} \Psi_i(p). \tag{26}$$

In the case of the SMPC algorithm, the DC voltages of connected areas are assumed constant. Finally, the CMPC cost is given by

$$J(k) = \sum_{i=1}^{N} J_i^{\rm local}(k). \tag{27}$$

7. Simulations

Simulations were carried out on a testbed, given in Fig. 1, previously developed in (Dai, 2011), to evaluate the performance of 6 different control algorithms for AGC using Matlab and Simulink. This system consists of 5 separate AC areas which are interconnected via a DC grid. The frequencies in the AC areas in this testbed are highly sensitive to load deviations, thus making it an interesting testbed for evaluating frequency control algorithms. The parameter values for the AC and DC grids are given in Table 1. For each simulation scenario the NVO and WVO strategies were evaluated for the PI, SMPC, and CMPC algorithms. Two different simulation scenarios were considered; in the first DC power regulation was enforced, and in the second it was not.

Table 1: AC and DC grid parameters (Dai, 2011).

AC grid parameters					
Area	1	2	3	4	5
$f_{\rm nom}$ (Hz)	50	50	50	50	50
$P_{\rm m}^0$ (MW)	50	80	50	30	80
$P_{\rm nom}$ (MW)	50	80	50	30	80
J (kg m^2)	2026	6485	6078	2432	4863
D_g (W s^2)	48.4	146.3	140	54.9	95.1
$T_{\rm sm}$ (s)	1.5	2.0	2.5	2	1.8
$P_{\rm l}^0$ (MW)	100.42	59.58	40.31	49.70	39.59
D_l (Hz^{-1})	0.01	0.01	0.01	0.01	0.01
$\bar{V}^{\rm dc}$ (kV)	99.17	99.6	99.73	99.59	100
$P^{\rm dc}$ (MW)	-50.4	20	10	-20	40.4
σ (no units)	0.02	0.04	0.06	0.04	0.03
γ (kV Hz^{-1})	2	2	2	2	2
$\tau_{\rm m}$ (s)	1.5	2	2.5	2	1.8
DC grid resistances (Ω)					
R_{12}	R_{15}	R_{23}	R_{25}	R_{34}	R_{45}
1.39	4.17	2.78	6.95	2.78	2.78

In the first scenario the control implication is that it is necessary for the area in which there is a fault to compensate for the fault in the long term using its local reserves. Thus, in the latter scenario it is of interest to see how well reserves are shared across areas using the different control approaches. For convenience, the $\eta_i = 0$ or 1 terminology, used for the PI controllers, will be used to denote whether DC power regulation is on or off, respectively.

The system was simulated for 80 s, and at time $t = 0$, $P_{\rm l2}^0$ was increased by 5% of its original value which necessitated responses from the primary and secondary frequency controllers in each area. The nonlinear system was simulated in discrete time with a sample step of $t_s = 0.01$ s using dynamic equations (1), (2), (3), (5), (9), and (22). Agents did not have access to disturbance measurements and so the controllers had to compensate for the unknown step disturbance and nonlinearities. It was assumed that measurements were noise free and that the system states were fully observable. Plots of the frequency responses and the DC power response for each area, for the case when there is only primary frequency control applied to both the mechanical power and DC voltages, are given in Figs. 3 and 4, respectively. Without any secondary control all the areas experience persistent long term errors in both the frequency and DC power responses.

Each agent in the MPC cases was given a $\tau_{\rm dc}$ time constant of 1 s. This gives a smooth response to the AGC HVDC controller and also ensures that the voltage predictions are accurate. For the purposes of minimisation of $\tilde{\boldsymbol{z}}_i$ in the SMPC case, agent i assumed that the DC voltages at HVDC connected areas were constant and maintained their initial values for the duration of the simulation.

The PI gains used in each area for the PI cases were $\chi_{{\rm m}i}$=0.03 and $\chi_{{\rm dc}i}$=0.005. A sample step of 0.2s was used

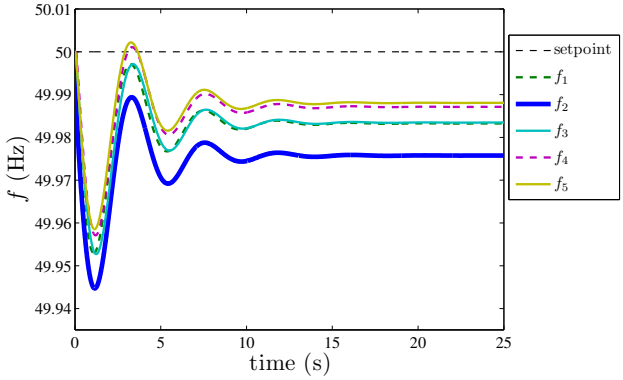

Figure 3: Plots of the frequencies in each area for the first 25 s of the simulation, when only the primary frequency controllers are operational.

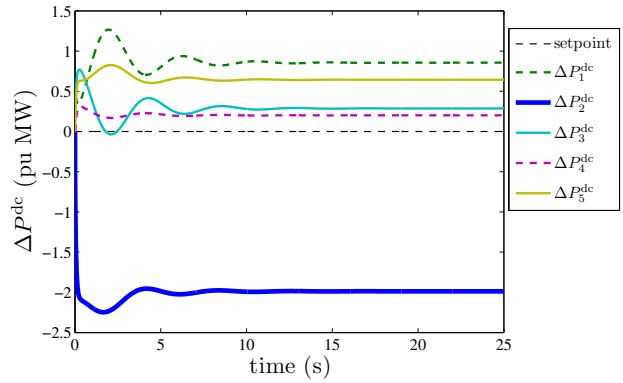

Figure 4: Plots of the DC power being injected into each area for the first 25 s of the simulation, when only the primary frequency controllers are operational.

for the discrete-time MPC controllers and the linear state-space equations for the system were discretised using a Zero Order Hold. The prediction horizon was chosen as $H = 50$. The weights for the MPC algorithms were given as follows: $Q_{\mathrm{f}i} = 1$, $Q_{\mathrm{z}i} = 0.001$, $Q_{\mathrm{df}i} = 1000$, $Q_{\mathrm{dP}i} = 1$, and $Q_{\mathrm{dv}i} = 1000$, for $i = 1, \ldots, 5$. All the above PI and MPC controller parameters were chosen so as to provide a good performance trade-off between the objectives of minimising frequency deviations, ROCOF, and power deviations when $\eta_i = 1$. It is acknowledged that a more comprehensive comparison would require optimisation of the PI gains and MPC weights with respect to an overall aggregate performance metric, e.g. the H_∞ tuning metric, but such optimisation is beyond the scope of this paper.

Metrics such as CPS1 and CPS2 and, the previously developed criteria A_1 and A_2, are used to measure the long term effictiveness of frequency control in power systems (Jaleeli and Vanslyck, 1999). However, given that deterministic sources and loads are considered in the simulations in this paper for identical fault scenarios, least squares metrics based on the control objectives are considered, as in (Venkat et al., 2008; Hermans et al., 2012; Negenborn et al., 2008). A number of different metrics are defined to compare the performance of the different algorithms numerically. The first 3 of these are the frequency tracking metric, $\mathcal{C}_{\mathrm{f}}{=}\sum_{k=1}^{k_f}\sum_{i=0}^{5} f_i^2(kt_s)$, the ROCOF metric $\mathcal{C}_{\mathrm{df}}{=}\sum_{k=0}^{k_f}\sum_{i=1}^{5}\Delta f_i^2(kt_s)$, and the DC power tracking metric $\mathcal{C}_{\mathrm{P}}{=}\sum_{k=0}^{k_f}\sum_{i=1}^{5}\Delta P_{\mathrm{dc}i}^2(kt_s)$, where k_f is the final simulation sample of the experiment. It is also desired to have a metric to determine how well reserves have been shared between areas over the course of the simulation. The maximum difference between the final values of $P_{\mathrm{m}i}$, $\mathcal{C}_{\mathrm{r}}{=}\max\left(P_{\mathrm{m}i}(k_f t_s) - P_{\mathrm{m}j}(k_f t_s)\right)$, for $j = 1, \ldots, 5$, $i = 1, \ldots, 5$, was thus used. Reduced values of this metric imply a better sharing of reserves across the entire grid, as in turn it implies the mechanical powers produced in each area are more similar. All the aforementioned metrics were calculated using pu values, where the base frequency, $f_{\mathrm{base}} = 50$ Hz, the base power, $P_{\mathrm{base}} = 100$ MW, and the base voltage, $V_{\mathrm{base}} = 100$ kV.

8. Results

Firstly, the results will be given for an experiment in which both the frequency and DC powers need to be regulated. In this first experiment it will be assumed that all system parameters are known exactly by the control agents. However, typically there is some uncertainty associated with the control agents' knowledge of the system parameters. Thus in the second part of this section the performance of controllers is tested for the case when there is parameter uncertainty, and it is desired to regulate both the frequency and DC powers again. Finally, the controllers are tested for the case where it is only desired to regulate the frequency. In particular, the sharing of reserves between areas is highlighted in this final set of results.

8.1. Simulation with $\eta_i = 1$

Figs. 5 and 6 show the frequency and DC power responses, respectively, for area 2 when $\eta_i = 1$, for $i = 1, \ldots, 5$. While Fig. 5 only focuses on the first 25 seconds of simulation, each controller succeeds in restoring the frequency in area 2 to its original setpoint within 80 seconds. The performance metrics for each of the controllers are given in Table 2.

It can be seen from the results that there are several advantages gained through the use of the MPC algorithms. The PI algorithms experience the largest initial frequency deviations, the SMPC algorithms have the smallest initial frequency deviation, and the CMPC algorithms give performance lying between these two. The CMPC algorithms achieve the best frequency damping and minimisation of ROCOF, but the PI and SMPC algorithms provide similar responses in this regard, with the SMPC algorithms

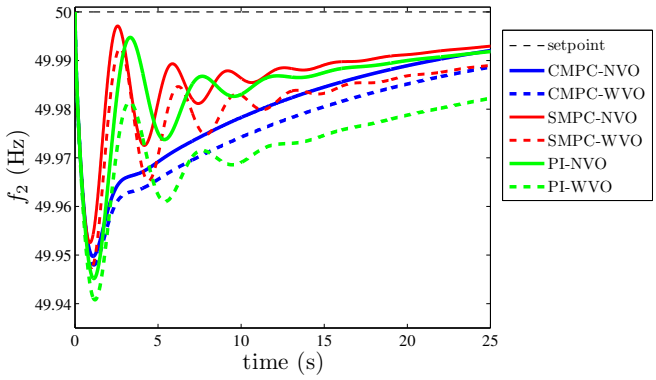

Figure 5: Plots of the frequencies in area 2 for the first 25 s of the simulation, when η_i=1, and under the various control schemes.

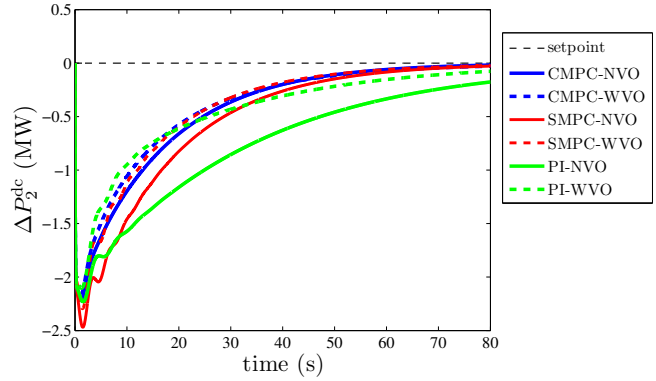

Figure 6: Plots of the DC power being injected by area 2 into the MTDC grid, when η_i=1, and under the various control schemes.

providing better $\mathcal{C}_{\mathrm{f}}$ performance and the PI providing better $\mathcal{C}_{\mathrm{df}}$ performance between the two decentralised algorithms. It should be noted at this point that minimisation of frequency deviations and ROCOF are conflicting objectives. By minimising the ROCOF, it implies that the frequency regulation is slowed down, thus as can be seen in Table 2, in the CMPC cases for example, improved ROCOF performance results in reduced frequency regulation performance.

The general trend here, with regards to the differences in performance between the NVO and WVO algorithms, is that there is a trade-off in performance between frequency and DC power tracking, with the NVO algorithms providing improved frequency regulation, and the WVO algorithms experiencing better DC power tracking. However, it is not obvious at this point as to what significant advantages the WVO algorithms provide over the NVO algorithms. These advantages are shown in the following two sections in terms of an improvement in performance when faced with parameter uncertainty, and with regard to the ability of the WVO algorithm to improve the capability of the overall system to share secondary reserves across the DC grid.

Table 2: Performance metrics for different control techniques based on 80 s simulations for $\eta_i = 1$, for $i = 1, \ldots, 5$ (the best result for each metric is highlighted using bold text).

Method	$\mathcal{C}_{\mathrm{f}}$ (10^{-4})	$\mathcal{C}_{\mathrm{df}}$ (10^{-8})	$\mathcal{C}_{\mathrm{P}}$ (10^{-1})
PI-NVO	9.8	8.9	9.9
PI-WVO	15.1	8.3	**4.4**
SMPC-NVO	**6.5**	9.1	7.2
SMPC-WVO	8.1	9.9	4.9
CMPC-NVO	17.7	5.15	5.5
CMPC-WVO	18.2	**5.09**	4.7

8.2. Evaluating the robustness of controllers to model uncertainty

The robustness of the controllers has been demonstrated in the last section with regards to the system's ability to overcome the effects of unknown disturbances and uncertainties related to the linearisation of the nonlinear model for control. In order to evaluate the robustness of the controllers with respect to parameter uncertainties, the values for J given in Table 1 are used for the control system design in the MPC cases but the values used in the simulation are scaled by $\rho_H = 0.7$. The values of R_{dc} in Table 1 are used for control in the MPC cases again, but the real values of R_{dc} are scaled by $\rho_R = 1.3$. In particular, the variation of R_{dc} affects the performance of the control system, as this effects not only the controller's performance from a parametric uncertainty perspective, but will also affect the system's original load flow calculations, resulting in unbalanced power flows in the system at the start of the simulation. The imbalances due to inaccurate load flow calculations are illustrated in Figs. 7 and 8, where it can be seen that significant long term deviations occur when only the primary frequency controllers are employed. It should be noted in these figures that no other external disturbance has been applied. In the following, the step load disturbance which was previously applied in area 2 is applied again as an additional disturbance source in evaluating the secondary controllers. Thus there is a significant level of uncertainty affecting the performance of the controllers.

The frequency response can be seen over the course of the full simulation in Fig. 9, and the initial transient response can be seen in greater detail for the first 10s of the simulation in Fig. 10, for area 1 (area 1 has the largest frequency deviations in this instance due to the unbalanced power flows). The DC power and DC voltage responses in area 1 can also be seen Figs. 11 and 12, respectively. The performance metrics for each controller are given in Table 3. From these results it can be seen that the use of the secondary voltage offsets significantly enhances the robustness of the responses. In each of the WVO cases both the frequency and DC power are returned to their desired setpoints, whereas the use of the NVO based controllers results in sustained frequency and DC power offsets, as can be seen in Fig. 9. This is because the NVO cases are

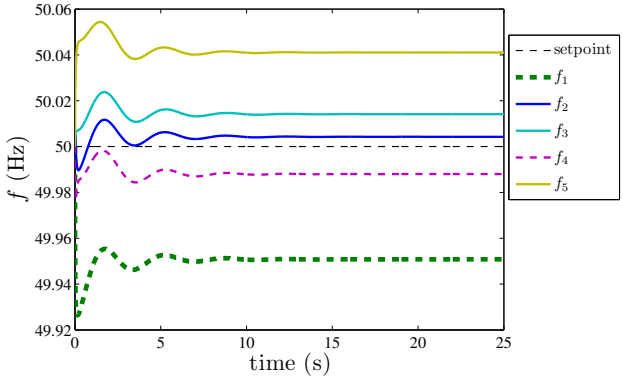

Figure 7: Plots of the frequencies in each area for the first 25 s of the simulation, when only the primary frequency controllers are operational, with $\rho_H = 0.7$ and $\rho_R = 1.3$. The deviations here are a result of the model uncertainty only.

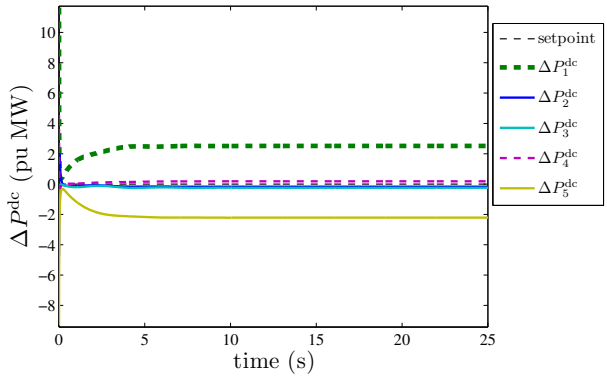

Figure 8: Plots of the DC power being injected into each area for the first 25 s of the simulation, when only the primary frequency controllers are operational, with $\rho_H = 0.7$ and $\rho_R = 1.3$. The deviations here are a result of the model uncertainty only.

based on creating voltage deviations about the original DC voltage operating point according the proportional control law given in (6), and so cannot re-establish a new operating point for the DC voltage to operate about. In the WVO case the additional voltage offsets allow the system to effectively realign the DC voltages about a new voltage operating point, about which the frequency and DC power can be regulated correctly.

Additionally, it can be seen that both the CMPC-WVO and SMPC-WVO approaches provide a significantly more robust response to the parameter variations than the PI-WVO approach. In particular, the PI-WVO algorithm experiences a larger initial frequency deviation than either of these algorithms, as can be seen in Fig. 10, and additionally experiences a larger ROCOF under parameter uncertainties than the other approaches, as can be seen in Table 3. Thus, in terms of the original tuning goals of trading off ROCOF and frequency regulation, based on the nominal system model, it could be concluded that the CMPC-WVO and SMPC-WVO approaches improve the

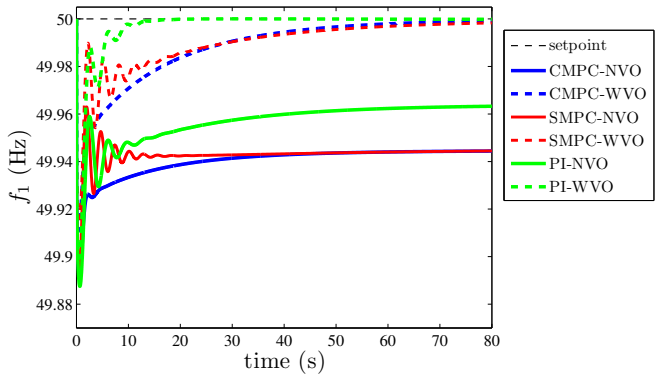

Figure 9: Plots of the frequencies in area 1 under model uncertainty, when η_i=1, with the various control schemes.

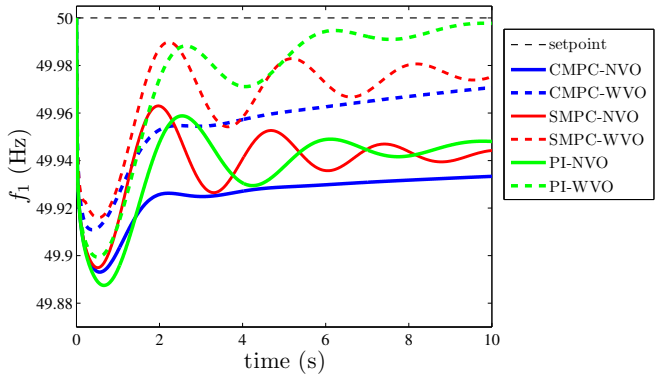

Figure 10: Plots of the frequencies in area 1 under model uncertainty, when η_i=1, with the various control schemes, for the first 10s of the simulation.

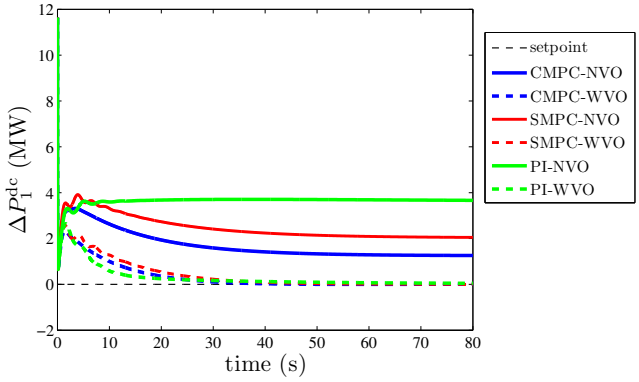

Figure 11: Plots of the DC power being injected by area 1 into the MTDC grid under model uncertainty, when η_i=1, and using the various control schemes.

robustness of the system in comparison to the PI-WVO approach. However, the PI-WVO does provide a more damped response than the SMPC-WVO response in area 1, as can be seen in Fig. 10, and provides a better overall frequency regulation cost than the CMPC-WVO, at the expense of the ROCOF/frequency trade-off, as can be seen in Table 3.

It should be noted that the improved robustness of

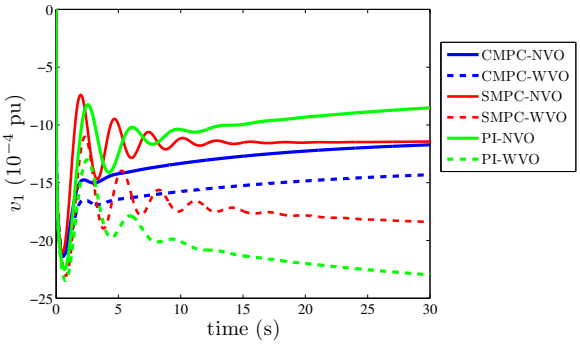

Figure 12: Plots of the DC voltages in area 1 under model uncertainty, when η_i=1, and using the various control schemes.

Table 3: Performance metrics for different control techniques based on 80 s simulations for $\eta_i = 1$, for $i = 1, \ldots, 5$, $\rho_H = 0.7$, and $\rho_R = 1.3$ (the best result for each metric is highlighted using bold text).

Method	$\mathcal{C}_{\mathrm{f}}$ (10^{-3})	$\mathcal{C}_{\mathrm{df}}$ (10^{-7})	$\mathcal{C}_{\mathrm{P}}$
PI-NVO	13.3	12.5	17.3
PI-WVO	2	12.25	0.7
SMPC-NVO	16.4	12.6	9.3
SMPC-WVO	**1.7**	9.2	0.91
CMPC-NVO	19.7	11.7	4.2
CMPC-WVO	2.5	**8.3**	**0.6**

MPC in comparison to PI under parameter uncertainty has been observed previously in AGC applications (Mohamed et al., 2011, 2012). Inbuilt integrators, iterative state measurements (Wang, 2009), and MPC's ability to use a range of state measurements, as opposed to only using the frequency and DC power measurements, allow MPC to overcome various uncertainties and provide improved robustness in comparison to PI based AGC.

8.3. Simulation with $\eta_i = 0$

The frequency response in area 2 when $\eta_i = 0$ (when the system parameters for control are accurately known once again), can be seen in Fig. 13. The performance metrics for this simulation are given in Table 4. Again, CMPC gives the best response in terms of damping, while the SMPC and PI algorithms give similar responses, as can be seen in Fig. 13. The WVO cases provide improved control performance versus the NVO cases in everything except the minimisation of ROCOF in the case of the SMPC-WVO algorithm, as can be seen in Table 4.

Of particular interest here is the improvement in terms of the system's ability to share long term reserves across the grid. In comparison with the NVO cases, the WVO algorithms enable a significant improvement in the sharing of resources over the grid. Figs. 14 and 15 show plots of the mechanical power deviations in each area with the PI controllers when $\eta_i = 0$, over a 500 s simulation. The PI-WVO results are depicted in Fig. 14 and the PI-NVO

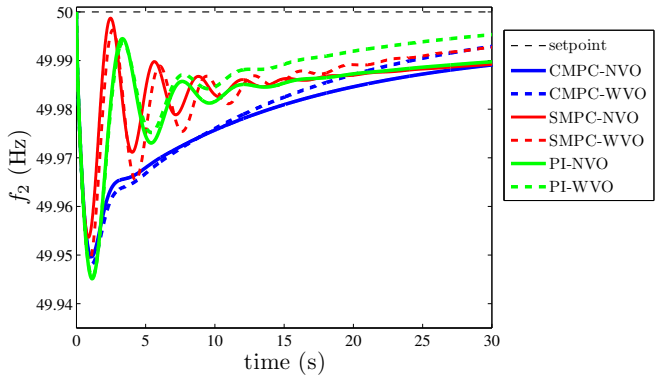

Figure 13: Plots of the frequencies in each area for the first 30 s of the simulation, when η_i=0, and under different schemes.

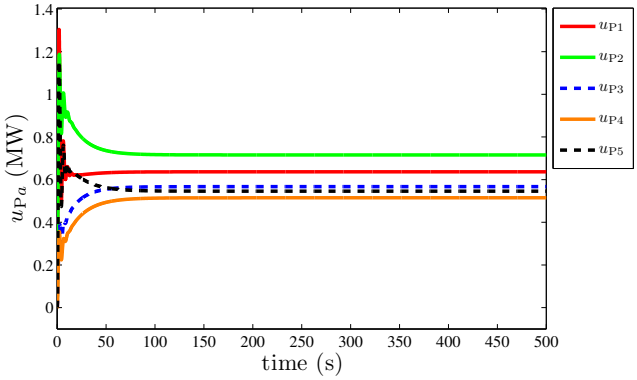

Figure 14: Plots of the mechanical powers generated in each area when secondary PI-based DC voltage offset control is enabled.

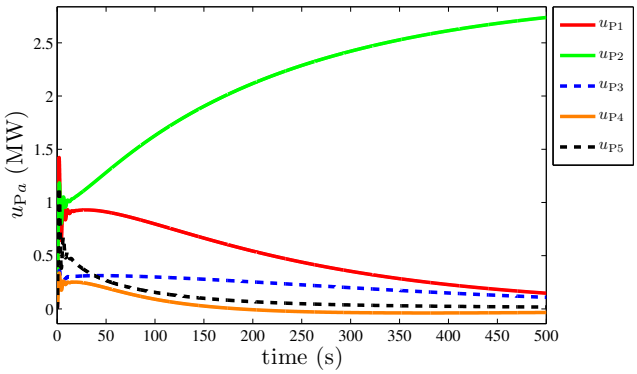

Figure 15: Plots of the mechanical powers generated in each area when secondary PI-based DC voltage offset control is disabled.

results in Fig. 15. It can be seen here that after the initial transient in the NVO case, area 2 predominantly satisfies its frequency regulation needs through local generation, while the other areas reduce their mechanical power outputs to the pre-disturbance levels with time. However, in the WVO cases each of the areas generates more mechanical power in order to act cooperatively to counteract area 2's disturbance, sharing their reserves more effectively across the grid.

While the PI case is used to illustrate the improved

Table 4: Performance metrics for different control techniques based on 80 s simulations for $\eta_i = 0$, for $i = 1, \ldots, 5$ (the best result for each metric is highlighted using bold text).

Method	$\mathcal{C}_{\mathrm{f}}$ (10^{-4})	$\mathcal{C}_{\mathrm{df}}$ (10^{-8})
PI-NVO	11.1	8.9
PI-WVO	10.8	8.5
SMPC-NVO	7.5	9.8
SMPC-WVO	**7.1**	11.2
CMPC-NVO	19.2	5.2
CMPC-WVO	17.9	**5.1**

Table 5: Performance metrics for different control techniques based on 500 s simulations (the best result is highlighted using bold text).

Method	PI-WVO	SMPC-WVO	CMPC-WVO
$\mathcal{C}_{\mathrm{r}}$ (10^{-3})	**2.01**	3.9	4.04

sharing of secondary resources here, improved sharing is observed for each of the other WVO cases with $\eta_i = 0$. The $\mathcal{C}_r$ values for each of the controllers are calculated for 500 s simulations in Table 5. Here it can be seen that the PI-WVO algorithm gives the best sharing of resources, with the MPC-WVO and SMPC-WVO algorithms giving similar results. The reason for the improvement in reserve sharing is similar to that given earlier for the improved robustness of the WVO cases; as the WVO cases allow a new voltage setpoint to be determined, it in turn means that the DC power entering or leaving an area can be changed over longer time scales, thus allowing increased sharing of reserves over the DC grid.

8.4. Discussion

From the results outlined in the previous subsections, the following can be observed:

- The use of voltage offsets provides significant advantages in terms of the performance of the system and its robustness to disturbances.
- The MPC-WVO and SMPC-WVO algorithms offer improved performance and robustness under parameter uncertainty over the PI-WVO algorithm.
- Provided that it is not desired to regulate DC powers to their scheduled values, the use of voltage offsets enables increased efficiency in the sharing of long term secondary reserves over the entire grid.

The main advantage of the PI-WVO algorithm is its decentralised architecture and simple structure. However, by employing the more complex decentralised SMPC controller the benefits of the decentralised PI can be improved upon, whilst making the system more robust to uncertainties. While the CMPC-WVO algorithm gives the best frequency-DC power regulation performance trade off, it may require a fast communications infrastructure over a large geographical area, in order to be implemented in reality, and it may not be possible to implement such a centralised control architecture when a number of Transmissions Systems Operators are responsible for different sections of interconnected AC or DC grids. The performance difference between the CMPC and SMPC algorithms motivates further work in the application of distributed MPC algorithms for this application, where agents could coordinate their responses through limited inter-TSO communication in order to improve performance.

It has been observed that in each of the WVO control configurations, the secondary reserves can be shared across the grid more effectively. Thus, in terms of the real-time market the use of DC voltage offsets could be useful in enabling the aggregation of renewable resources across a wide area. This in turn could help counteract the negative effects associated with large penetrations of renewables in a given area.

The results in Figs. 14 and 15 also have implications for the recently published EU policy on renewables for 2030 (European Commission, 2014). For the 2020 targets, each individual country was tasked with achieving a 20% renewables penetration target within that country. Hence, from a secondary reserves perspective, the incentive is for countries to provide long term reserves locally within that country, and so the response in Fig. 15 is more desirable, in terms of local renewable sources being used. It should be noted that when $\eta_i = 1$ in an area it will also produce the secondary reserves locally. Policy has changed for the 27% target in 2030, where a 27% renewables penetration is to be achieved collectively across Europe. Thus the response in Fig. 14 would be more desirable where countries collectively contribute to AGC across the entire grid. Therefore, the use of voltage offsets as part of AGC implementations could be useful in satisfying these policy objectives.

9. Conclusion

In this paper a number of decentralised and centralised PI and Model Predictive Control (MPC) based algorithms were proposed for the purposes of Automatic Generation Control (AGC) in Multi-Terminal HVDC (MTDC) grids. The use of voltage offsets was also proposed as an additional control variable to improve performance. Each of these algorithms provided stabilising control, and the advantages and disadvantages of the various algorithms were discussed in detail. Of note was the fact that the use of voltage offsets in AGC allowed for reserves to be shared across the grid in a more efficient manner over longer time scales.

Future work will consider the application of distributed control algorithms for AGC in MTDC grids, as well as incorporating system constraints and stochastic uncertainties into the control formulation. It is also of interest to consider ways of using MPC to trade off the competing objectives of keeping power transfers on the DC network

at given levels, while at the same time trying to share resources, and to consider networks in which there are parallel AC and DC interconnections.

Acknowledgment

Paul Mc Namara, Seán McLoone and Terence O'Donnell are funded by Science Foundation Ireland as part of the Sustainable Electrical Energy Systems (SEES) Research Cluster (grant 09/SRC/E1780). Ronan Meere is funded under the Programme for Research in Third Level Institutions and co-funded under the European Regional Development Fund (ERDF).

Andreasson, M., Nazari, M., Dimarogonas, D., Sandberg, H., Johansson, K., Ghandhari, M., August 2013. Distributed voltage and current control of multi-terminal high-voltage direct current transmission systems. In: Proceedings of the 19th IFAC World Congress. Cape Town, South Africa.

Arags-Pealba, M., Egea-lvarez, A., Galceran Arellano, S., Gomis-Bellmunt, O., 2014. Droop control for loss minimization in HVDC multi-terminal transmission systems for large offshore wind farms. Electric Power Systems Research 112 (0), 48 – 55.

Azad, S., Iravani, R., Tate, J., Aug 2013. Damping Inter-Area Oscillations Based on a Model Predictive Control (MPC) HVDC Supplementary Controller. IEEE Transactions on Power Systems 28 (3), 3174–3183.

Beerten, J., Belmans, R., Nov. 2013. Analysis of Power Sharing and Voltage Deviations in Droop-Controlled DC Grids. IEEE Transactions on Power Systems 28 (4), 4588–4597.

Chaudhuri, N., Chaudhuri, B., Majumder, R., Yazdani, A., 2014. Multi-terminal Direct-current Grids: Modeling, Analysis, and Control. John Wiley & Sons.

Chaudhuri, N., Majumder, R., Chaudhuri, B., 2013. System Frequency Support Through Multi-Terminal DC (MTDC) Grids. IEEE Transactions on Power System 28 (1), 347–356.

Dai, J., 2011. Frequency control coordination among non-synchronous AC areas connected by a multi-terminal HVDC grid. Ph.D. thesis, Supélec, France.

Dai, J., Phulpin, Y., Sarlette, A., Ernst, D., 2010. Impact of delays on a consensus-based primary frequency control scheme for AC systems connected by a multi-terminal HVDC grid. In: Proceedings of the iREP Symposium on Bulk Power System Dynamics and Control. pp. 1–9.

Dai, J., Phulpin, Y., Sarlette, A., Ernst, D., 2012. Coordinated primary frequency control among non-synchronous systems connected by a multi-terminal high-voltage direct current grid. IET Generation, Transmission, Distribution 6 (2), 99–108.

de Courreges d'Ustou, B., 2012. Optimal Control Design For Multi-terminal HVDC. Ph.D. thesis, University of Pittsburgh.

Egea-Alvarez, A., Beerten, J., Van Hertem, D., Gomis-Bellmunt, O., Dec 2012. Primary and secondary power control of multiterminal HVDC grids. In: Proceedings of the 10th IET International Conference on AC and DC Power Transmission. pp. 1–6.

Egea-Alvarez, A., Bianchi, F., Junyent-Ferre, A., Gross, G., Gomis-Bellmunt, O., 2013. Voltage Control of Multiterminal VSC-HVDC Transmission Systems for Offshore Wind Power Plants: Design and Implementation in a Scaled Platform. IEEE Transactions on Industrial Electronics 60 (6), 2381–2391.

Ersdal, A., Imsland, L., Uhlen, K., 2016. Model predictive load-frequency control. IEEE Transactions on Power Systems 31 (1), 777–785.

Ersdal, A. M., Imsland, L., Uhlen, K., Fabozzi, D., Thornhill, N., 2015. Model predictive load frequency control taking into account imbalance uncertainty. in press with Control Engineering Practice.

European Commission, 2014. A policy framework for climate and energy in the period from 2020 to 2030.

Fuchs, A., Imhof, M., Demiray, T., Morari, M., 2014. Stabilization of large power systems using VSC–HVDC and model predictive control. IEEE Transactions on Power Delivery 29 (1), 480–488.

Hendriks, R., Paap, G., Kling, W., May 7–10 2007. Control of a multiterminal VSC transmission scheme for connecting offshore wind farms. In: Proceedings of the European Wind Energy Conference Exhibition. Milan, Italy, p. 8.

Hermans, R., Jokić, A., Lazar, M., Alessio, A., Van den Bosch, P., Hiskens, I., Bemporad, A., 2012. Assessment of non-centralised model predictive control techniques for electrical power networks. International Journal of Control 85 (8), 1162–1177.

Houghton, T., Bell, K., Doquet, M., 2012. The economic case for developing HVDC-based networks to maximise renewable energy utilisation across Europe: an advanced stochastic approach to determining the costs and benefits. CIGRE.

Jaleeli, N., Vanslyck, L., Aug 1999. NERC's new control performance standards. IEEE Transactions on Power Systems 14 (3), 1092–1099.

Kundur, P., 1994. Power System Stability and Control. Mc-Graw Hill, New York.

Ma, M., Chen, H., Liu, X., Allgöwer, F., 2014. Distributed model predictive load frequency control of multi-area interconnected power system. International Journal of Electrical Power & Energy Systems 62, 289 – 298.

Maciejowski, J., 2002. Predictive Control with Constraints. Prentice Hall, Harlow, England.

Mariethoz, S., Fuchs, A., Morari, M., Feb. 2014. A VSC-HVDC Decentralized Model Predictive Control Scheme for Fast Power Tracking. IEEE Transactions on Power Delivery 29 (1), 462–471.

Mc Namara, P., Meere, R., O'Donnell, T., McLoone, S., August 2014. Distributed MPC for Frequency Regulation in Multi-Terminal HVDC Grids. In: Proceedings of the IFAC World Congress. Cape Town, South Africa.

Mohamed, T., Morel, J., Bevrani, H., Hiyama, T., 2012. Model predictive based load frequency control design concerning wind turbines. International Journal of Electrical Power & Energy Systems 43 (1), 859 – 867.

Mohamed, T. H., Bevrani, H., Hassan, A. A., Hiyama, T., 2011. Decentralized model predictive based load frequency control in an interconnected power system. Energy Conversion and Management 52 (2), 1208–1214.

Negenborn, R. R., De Schutter, B., Hellendoorn, J., April 2008. Multi-agent model predictive control for transportation networks: Serial versus parallel schemes. Engineering Applications of Artificial Intelligence 21 (3), 353–366.

Sarlette, A., Dai, J., Phulpin, Y., Ernst, D., 2012. Cooperative frequency control with a multi-terminal high-voltage DC network. Automatica 48 (12), 3128 – 3134.

Shiroei, M., Ranjbar, A., 2014. Supervisory predictive control of power system load frequency control. International Journal of Electrical Power & Energy Systems 61, 70 – 80.

Shiroei, M., Toulabi, M., Ranjbar, A., 2013. Robust multivariable predictive based load frequency control considering generation rate constraint. International Journal of Electrical Power & Energy Systems 46, 405 – 413.

Silva, B., Moreira, C., Seca, L., Phulpin, Y., Peas Lopes, J., 2012. Provision of Inertial and Primary Frequency Control Services Using Offshore Multiterminal HVDC Networks. IEEE Transactions on Sustainable Energy 3 (4), 800–808.

Spro, O. C., Torres-Olguin, R. E., Korps, M., 2014. North sea offshore network and energy storage for large scale integration of renewables. accepted for publication in Sustainable Energy Technologies and Assessments.

Tang, G., He, Z., Pang, H., Huang, X., Zhang, X.-P., 2015. Basic topology and key devices of the five-terminal DC grid. CSEE Journal of Power and Energy Systems 1 (2), 22–35.

Tielens, P., Van Hertem, D., April 2012. Grid Inertia and Frequency Control in Power Systems with High Penetration of Renewables. In: Proceedings of the Young Researchers Symposium in Electrical Power Engineering. Delft, The Netherlands.

Van Hertem, D., Ghandhari, M., 2010. Multi-terminal VSC HVDC

for the European supergrid: Obstacles. Renewable and sustainable energy reviews 14 (9), 3156–3163.

Venkat, A., Hiskens, I., Rawlings, J., Wright, S., Nov. 2008. Distributed MPC Strategies With Application to Power System Automatic Generation Control. IEEE Transactions on Control Systems Technology 16 (6), 1192–1206.

Wang, D., Glavic, M., Wehenkel, L., 2014. Comparison of centralized, distributed and hierarchical model predictive control schemes for electromechanical oscillations damping in large-scale power systems. International Journal of Electrical Power & Energy Systems 58, 32 – 41.

Wang, L., 2009. Model Predictive Control System Design and Implementation Using Matlab. Advances in Industrial Control. Springer, London.

Wiget, R., Andersson, G., Andreasson, M., Dimarogonas, D., Johansson, K., June 2015. Dynamic simulation of a combined AC and MTDC grid with decentralized controllers to share primary frequency control reserves. In: Proceedings of the IEEE PowerTech conference. pp. 1–6.

Zonetti, D., Ortega, R., Benchaib, A., 2014. Modeling and Control of High-Voltage Direct-Current Transmission Systems: From Theory to Practice and Back. arXiv preprint arXiv:1406.4392.